Journal of Superconductivity and Novel Magnetism
https://doi.org/10.1007/s10948-020-05465-7

ORIGINAL PAPER

3D Finite Element Electromagnetic Analysis of a 14-Strand HTS Roebel Cable

S. Gijoy[1] · K. E. Reby Roy[1]

Received: 24 December 2019 / Accepted: 19 February 2020

Abstract
Roebel cables with HTS strands exhibit reduced AC losses and possess large current carrying capacity. Even though works on several 2D and 3D numerical modelling and simulations are available, little efforts are made on computer-aided design (CAD) modelling, finite element analysis (FEA) and simulation of Roebel strands and cables. In this paper, finite element electromagnetic analysis and simulations of a 14-strand HTS Roebel cable is performed. The results obtained are then compared with another work which uses an H-formulation technique to model the problem. Although several numerical simulations have been carried out to optimise the HTS Roebel cable, no FEA work has yet been conducted on the complete 3D structure of Roebel cable. This work can therefore be considered as an initiator of the 3D finite element electromagnetic analysis of HTS Roebel cables.

Keywords Finite element analysis · HTS · Roebel cable · Twisted strand · AC loss

1 Introduction

High-temperature superconductivity (HTS) was found in cuprates in the late twentieth century. Since then, a variety of cable geometries incorporated HTS layer, among them, Roebel structure exhibits both high current density and low AC loss. The geometry possessed by Roebel cable helps to attain full transposition of every strand in it; thus, an equal current will be shared by each strand, which in turn helps in reducing the AC loss and increased stability of the cable [1, 2]. Roebel cables with HTS layer in strands can carry significant current and achieve high current density and better transposition among strands [3]. However, the widespread application of Roebel concept is restricted by the technical drawbacks such as high production cost (because half the material is punched off and thrown away for making individual strands) and difficulty in producing long-length cables [4]. The non-uniformity of the tape's critical current, strand misalignment [5] and limited in-plane bending capability is another problem faced by Roebel cables [6, 7]. In the study conducted by [3], it was shown that transverse loading induce uneven and localised stress distribution in Roebel strands which may lead to rapid mechanical failure.

Notable benefits of the new generation HTS tapes are reduced AC losses, low production cost and extraordinary high critical currents. An effective way to reduce AC loss of 2G HTS tapes using soldered-stacked-square (3S) wire was reported in [8]. Experiments have shown that a 36-turn solenoid coil wound with 3S wire can reduce AC loss up to 80% compared with a coil wound commercial 2G HTS tape. The fabrication method, structure, electrical properties, advantage and mechanical characteristics of 3S wire are presented in the paper [9]. A few years ago, hydrogen sulphide–based superconductors with transition temperatures up to 80 K were also discovered [10]. The work done by [11] states that lanthanum hydride show superconductivity under a pressure of 170 GPa at 250 K, which is considered to be the highest temperature of superconductivity currently seen for any material. Technological advancement in the field of superconductivity has proven that HTS tapes can be used commercially and successfully in high-power machines, superconducting magnets and similar high-power applications. Such a successful milestone achievement is reported in the paper [12] in which the design, development and field testing of world's first rare-earth barium copper oxide (ReBCO) HTS rotor for a 3.6-MW wind generator is presented.

✉ S. Gijoy
gijoys@sctce.ac.in

K. E. Reby Roy
rebyroy@tkmce.ac.in

[1] Department of Mechanical Engineering, TKM College of Engineering, Kollam, Kerala, India

Published online: 26 February 2020

Since the role of HTS tapes in future practical applications is important, it is necessary to utilise the advantages of 3D FEA methods that can simulate the physical, magnetic and electrical characteristics of various HTS cables which helps in designing and developing advanced cables. In this work, for the analysis, Roebel cable was selected as limited authors performed 3D finite element analysis on this cable due to its complexity in modelling. Several works have been published under the area 3D simulation of Roebel cables, but each one has its limitations. The paper [13] presented a 3D time-dependent electromagnetic model of a 14-strand Roebel cable and its AC loss analysis. They considered both transport current and magnetisation situation and also mentioned the limitations of thin strip approximation method. The model used in [13] was the H-formulation, often used for 2D problems and the strand was modelled by considering only the HTS layer, which is surrounded by air. However, the model ignored the strand's natural twist which occurs during cable manufacturing. This small distortion may arise due to the transposition of one strand over the other, which can be noted from Fig. 1. Also in [13], in order to cut down the total degrees of freedom in the air domain, the HTS layer thickness was scaled to 10 μm. However, a real Roebel strand consists of copper stabilising layers, silver layers, HTS, buffer layer and substrate [14].

In this work, the AC loss analysis, the current distribution in strands and the magnetic field distribution are evaluated in a 14-strand HTS Roebel cable using finite element method in two cases: (i) AC magnetic field applied to HTS Roebel cable and (ii) AC passes through HTS Roebel cable. The results are then compared with the numerical results presented in [13]. For obtaining a comparable result, no wide variations are made on the boundary conditions and the geometry described in it. However, the present study takes into account the natural twist of the strand and no scale down is considered for the HTS layer thickness. The obtained results are also compared with already published results in [13, 15], which shows a similar trend.

Although several numerical simulations have been carried out to optimise the HTS Roebel cable, no work has yet been developed for the 3D finite element analysis and simulation of the complete 3D cable structure. This work can therefore be considered as an initiator for the 3D finite element electromagnetic analysis of HTS Roebel cables. Even though FEA has several advantages, limited authors analysed superconducting cables using this tool due to lack of property values in superconducting states. The main aim of this work is to exploit the advantages of using FEA in the electromagnetic analysis of various superconducting cables. Thus, we can predict all losses, visualise the distribution of current and magnetic field incurred with these types of cables in a better way.

2 Model Description

In this work, the 3D structure of Roebel strand and the cable is modelled using SOLIDWORKS 2014. The specification and parameters for modelling the strand and cable were adopted from [13]. The actual 3D structure of the Roebel cable is shown in Fig. 1 and the 2D representation consisting of only three strands is presented in Fig. 2. The notations used in Fig. 2 is mentioned in Table 1.

Practically, Roebel strands are produced by mechanical cutting of thin HTS-coated conductors into Roebel-shaped strands [2]. The structure of commercially available long-length YBCO-coated conductor tape, manufactured by SuperPower Inc., is shown in Fig. 3, which consists of copper stabiliser, silver overlayer, (RE)BCO HTS, buffer layers and the substrate.

The numerical analysis of HTS Roebel strand was already studied and presented in [13, 15–17] and several other papers. In all these works, numerical modelling and simulation were done by considering it as a straight conductor and overlooked the exact design parameters. However, while winding the strand into a cable, there will be a natural twist occurring due to the transposition of one strand over the other [16]. The present work has carefully studied all the design parameters and specifications of the real 2G HTS tape and Roebel strand and took a model that is very close to the exact dimension for electromagnetic analysis.

Figure 4 shows a Roebel strand detached from a 14-strand cable whose specification is given in Table 1. The typical twisting of the strand can be seen clearly in this figure. Modelling of the real case Roebel cable is done in such a

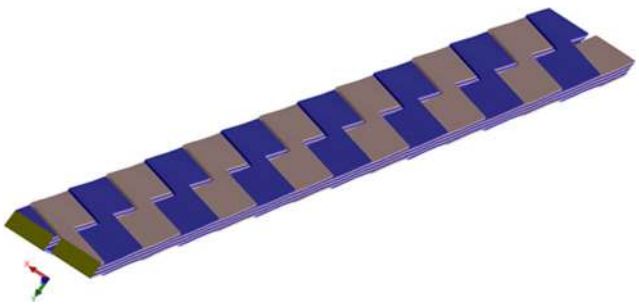

Fig. 1 A 14-strand Roebel cable modelled in SOLIDWORKS 2014. The length of one transposition is shown

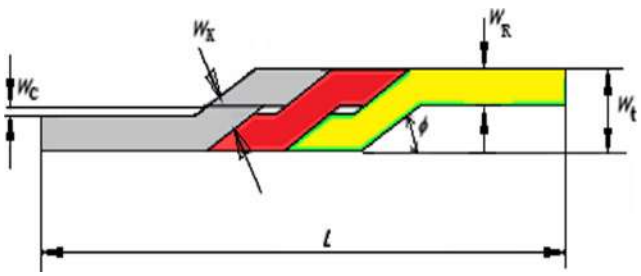

Fig. 2 2D representation of the transposition section of a three-stranded Roebel cable

Table 1 Specifications of the Roebel cable

Parameters	Values
Width of the tape (W_t)	4.3 mm
Strand width of straight section (W_R)	2 mm
Strand width at transposition section (W_x)	2 mm
Thickness of Hastelloy substrate	50 μm
Thickness of superconducting layer	1 μm
Thickness of copper stabilisation layer (on each side)	20 μm
Thickness of silver over layer (on each side)	2 μm
Gap between stacks of strands in the straight section (W_c)	0.3 mm
Transposition length (cabling pitch) (L)	109 mm
Roebel angle (φ)	35°
Number of strands	14
Total thickness of Roebel strand (approx.)	0.1 mm

way that all crossover regions of the strands may align in the same plane.

Figure 5 displays the overlapping of three strands. From this figure, one can ensure the orientation, position and how a strand goes into and from another strand, i.e. the meander structure of Roebel cable. It can be noted that the strand in a cable is not straight but got a small twist at the region where the transposition of the next strand occurs, which is indicated in Fig. 6.

When an AC supply is given to the Roebel cable, the entire current shared to a strand passes through the HTS due to its high conductivity [13]. Therefore, in the 3D model, the current work considered only the HTS layers and the surrounding air to reduce the load on the computer. The cable structure creates a repetitive region due to the transposition of strands in the Roebel cable, which helps to reduce the computational effort by considering a small region for the analysis. The geometry taken for analysis is shown in Fig. 7.

The analysis is first performed by considering the strand in the Roebel cable as straight, and the obtained result is then compared with [13]. The same analysis is also done on a real case Roebel cable that takes into account the natural twist of the strand. Both results are then compared to represent the

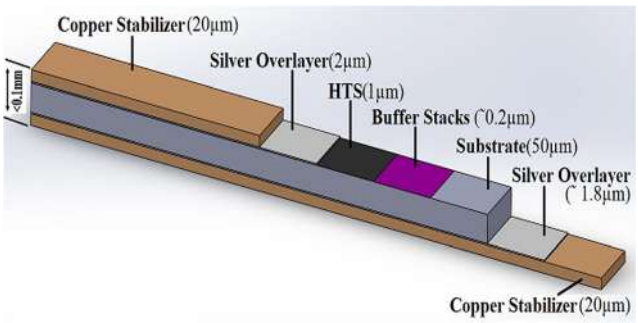

Fig. 3 The structure of the 2G HTS wire (modelled in SOLIDWORKS 2014) developed by SuperPower Inc. [2, 14, 15]

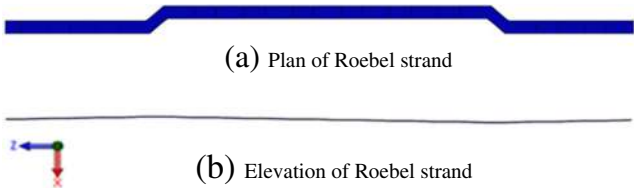

Fig. 4 Sketch of a Roebel strand isolated from a 14-strand cable. Two different orientations are shown. **a** Plan of Roebel strand. **b** Elevation of Roebel strand

influence of the twisting of the strand on AC loss, current distribution and magnetic flux density profile. In the entire literature, the Roebel cable with straight strands and the cable with strand's natural twisting considered is named simply as Roebel cable and real case Roebel cable respectively.

3 Boundary Conditions and Material Properties

The current can be supplied to the cable in different methods: constraining the current only in a single strand, constraining the current in all 14 strands of Roebel cable individually and constraining the current in all strands collectively. All the methods lead to a similar result [13]. In this work, the analysis considers the latter method. The various types of AC losses incurred in a Roebel cable while transferring current through it are hysteresis losses, eddy current losses, coupling losses and ferromagnetic losses. Among these losses, a significant portion of the AC loss in HTS Roebel cables is hysteresis loss [18]. The different types of losses occurring at each layer of the HTS Roebel cable are described in [19], and it is stated that the loss associated with superconducting HTS layer is only hysteresis loss. Therefore, only hysteresis losses are considered in this work while calculating the AC losses, as the proposed geometry only considers the HTS layer for electromagnetic analysis. It is noted that loss due to hysteresis would be much more significant than coupling loss if we apply an AC magnetic field perpendicular to the broad face of a Roebel cable [20]. Therefore, in the present work on the magnetization case, only the loss of hysteresis is considered to account for the total AC loss.

Fig. 5 3D representation of the transposition section of three Roebel strands

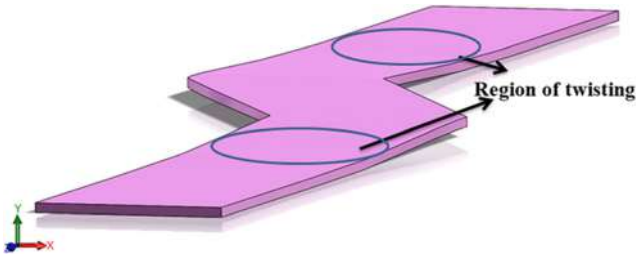

Fig. 6 Transposition section of a Roebel strand with natural twisting

In the paper [13], it is assumed that the current is distributed equally in all strands and the critical current of the cable is 465 A. The frequency of the applied current is set to 50 Hz and the influence of displacement current and eddy effects are neglected. The AC loss is also estimated for a varying magnetic field of 50 Hz from 0.01 to 0.1 T in a direction perpendicular to the broad face of the Roebel cable. The present work takes into account the same considerations and data.

In this paper, the HTS material is taken as $YBa_2Cu_3O_{7-\delta}$, whose density is 6300 kg/m^3 [21]. For the initial analysis, it is assumed that the material is isotropic and the relative permeability and permittivity are linear. The material properties corresponding to 77 K are taken for analysis. The relative permittivity of $YBa_2Cu_3O_{7-\delta}$ is taken from [22] which studied the technological development of using YBCO film for the manufacture of microwave filters. We know that the relative permeability of a material is susceptibility plus one. Several authors investigated the magnetic susceptibility of $YBa_2Cu_3O_{7-\delta}$ at cryogenic temperature [22, 23]. In the current work, the magnetic susceptibility and relative permeability of $YBa_2Cu_3O_{7-\delta}$ were taken from [24, 25] respectively.

The finite element electromagnetic analysis of the modelled 14-strand Roebel cable is performed using Ansys 2019 in which a perfect conductor material threshold is assigned; the electrical conductivity of $YBa_2Cu_3O_{7-\delta}$ is assigned a value just below that.

Mesh convergence and refinement study was carried out, and the optimum number of elements and size has been found out. Each strand of the Roebel cable has meshed with 3D tetrahedral elements. The continuum has discretised into 2,46,878 number of elements.

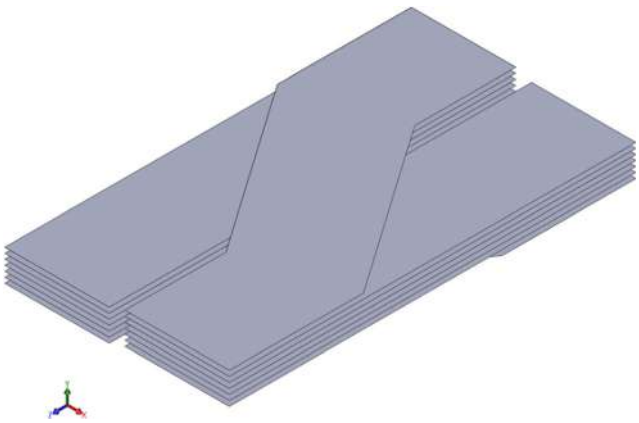

Fig. 7 Periodic section of a 14-strand Roebel cable taken for analysis

4 Results and Discussions

Finite element electromagnetic analysis and simulations are performed in two test cases: (i) Roebel cable exposed to a perpendicular magnetic field along the width of the cable and (ii) Roebel cable carrying transport current. The obtained results are then compared with the numerical results presented in [13]. The results are also compared with the output from the finite element electromagnetic analysis of a real case Roebel cable that takes into account the natural twist of the strand. Even though the analysis considers all 14 strands in the Roebel cable, the current density distribution pattern is expressed only in a single strand for getting clarity in visualisation. However, the AC loss pattern is shown in the full domain taken for analysis.

4.1 Magnetisation

An AC magnetic field varying from 0.01 to 0.1 T is applied to the broad face of the 14-strand Roebel cable and a plot showing the estimated AC loss vs applied magnetic field is given in Fig. 8.

A comparison between the estimated AC loss through finite element electromagnetic analysis with respect to the numerical analysis mentioned in [13] and the experimental data obtained from [15] is shown in Fig. 8. The graph is plotted in log scale in order to represent the minute variation of losses at very low magnetic field. The average of the analysed data obtained from the simulation against each applied magnetic

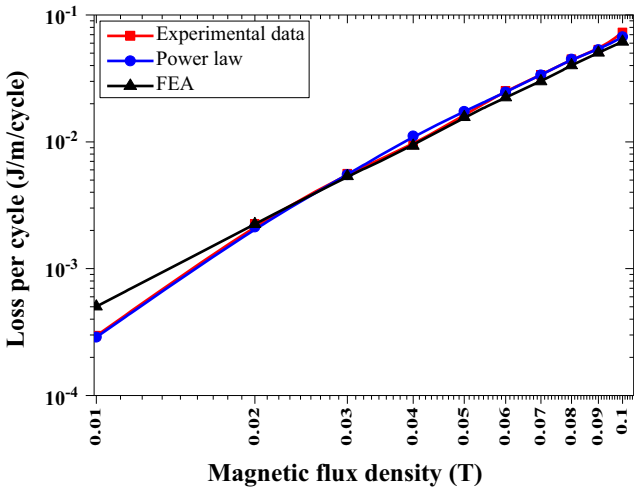

Fig. 8 Comparison shows the AC loss data (for magnetisation case) obtained from various authors with respect to the FEA explained in this work. Experimental data were obtained from [15]. The curve marked by power law is the data obtained from [13]

field is taken for plotting the graph in the FEA case. It is to be noted that the FEA results underestimate the power law only at a very low magnetic field. From 0.02 to 0.1 T, no significant variation is found between the results. Even though minute variation is noted between the experimental data, power law and FEA, the overall trend is reproduced. The main reason for deviation is because, in the experiment, the cable considers all the layers in it for calculating the loss and the frequency of the applied magnetic field was 72 Hz. However, in FEA, the loss is estimated only for the HTS layers and the strands are isolated individually, which the experiment overlooked. This can be attributed to a corresponding variation as other forms of losses such as eddy current loss in the stabilising layer and ferromagnetic loss in the substrate can contribute to the total AC loss [19].

The surface plot of the AC loss distribution in the domain of the 14-strand Roebel cable taken for analysis at an applied magnetic field of 0.05 T and 50 Hz is shown in Fig. 9.

From Fig. 9, it can be visualised that the AC loss is concentrated at the crossover region of the strand (i.e. at the transposition section), and the losses in the straight sections of the strand are almost the same. It is to be noted that for an applied field of 0.05 T, the maximum loss is 2.6E−02 J/m/cycle and the average loss is 1.60E−02 J/m/cycle which is almost similar to the data mentioned in [13]. For all applied magnetic fields from 0.01 to 0.1 T, the surface plot of the AC loss is the same; the only variation is observed in the magnitude of the obtained AC loss.

The same procedure, assumptions and boundary conditions have been taken for the finite element electromagnetic analysis of the Roebel cable which considers the strand's natural twist. The geometry of the domain taken for analysis is shown in Fig. 10.

Figure 11 shows the comparison between the AC loss data obtained from the analysis of the Roebel cable with straight strands and the Roebel cable with strand's natural twist considered. The average of the analysed data obtained from the simulation against each applied magnetic field, which varies from 0.01 to 0.1 T, is taken for comparison. The figure shows that the variation in AC loss between both cases is negligible. It is also noticed that the surface plot of the AC loss obtained at all applied magnetic fields in both cases is also similar.

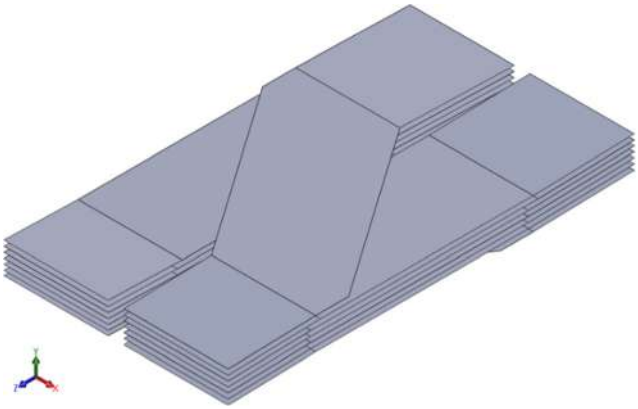

Fig. 10 The periodic section of the 14-strand Roebel cable in which the strand's natural twist is considered

The surface plot of the current density distribution in a 14-strand Roebel cable for an applied filed of 0.05 T is represented in figure 12. Analysing Fig. 12, one can note that the current density is high at the edge of the strand and also at the crossover region of the strand. The plot obtained is similar to that mentioned in [13]. Similar plots are evaluated for all applied fields (i.e. from 0.01 to 0.1 T); however, there are no variations in the distribution profile, except for the magnitude of the current density, which varies depending on the applied field.

The surface plots of the current density distribution profile at all different magnetic fields are also analysed for the real case Roebel cable. The plots show a similar impression with the only variation in the maximum current density. It is observed that while considering the natural twisting of the

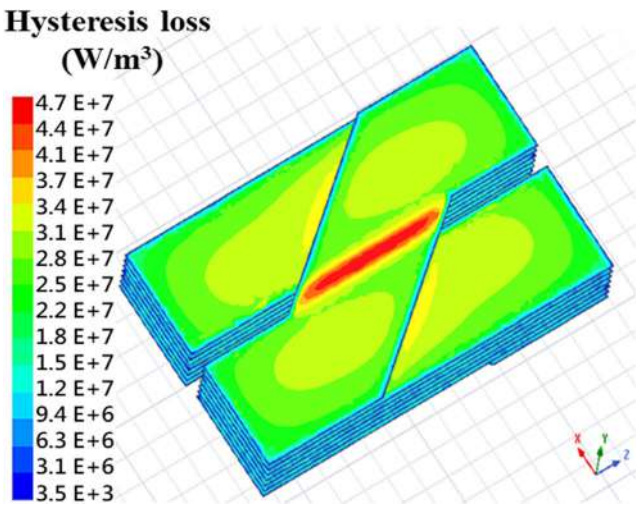

Fig. 9 Surface plot of the distribution of AC loss in a 14-strand Roebel cable at an applied magnetic field of 0.05 T

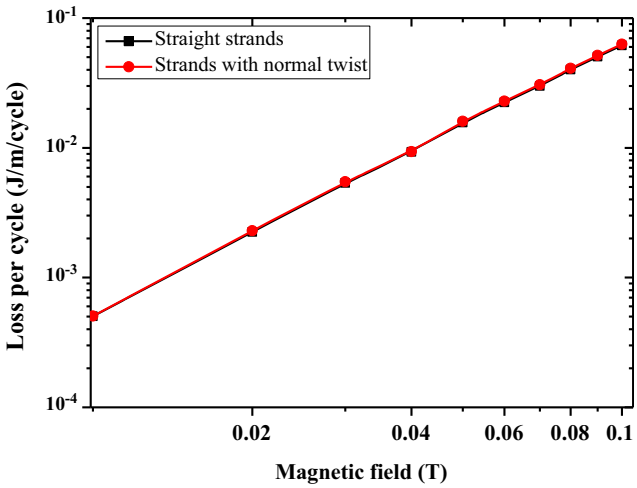

Fig. 11 Plot showing the comparison between the AC losses in the Roebel cables that ignored the strand's natural twisting and that considered the strand's natural twisting

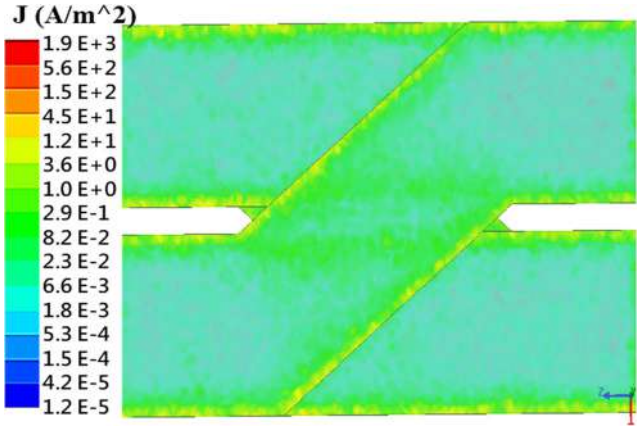

Fig. 12 Surface plot of the current density distribution in a 14-strand Roebel cable for an applied field of 0.05 T

strand, the maximum current density of the Roebel cable for an applied magnetic field increases. The magnetic field distribution around the region of the Roebel cable for an applied field of 0.05 T is plotted and presented in Fig. 13.

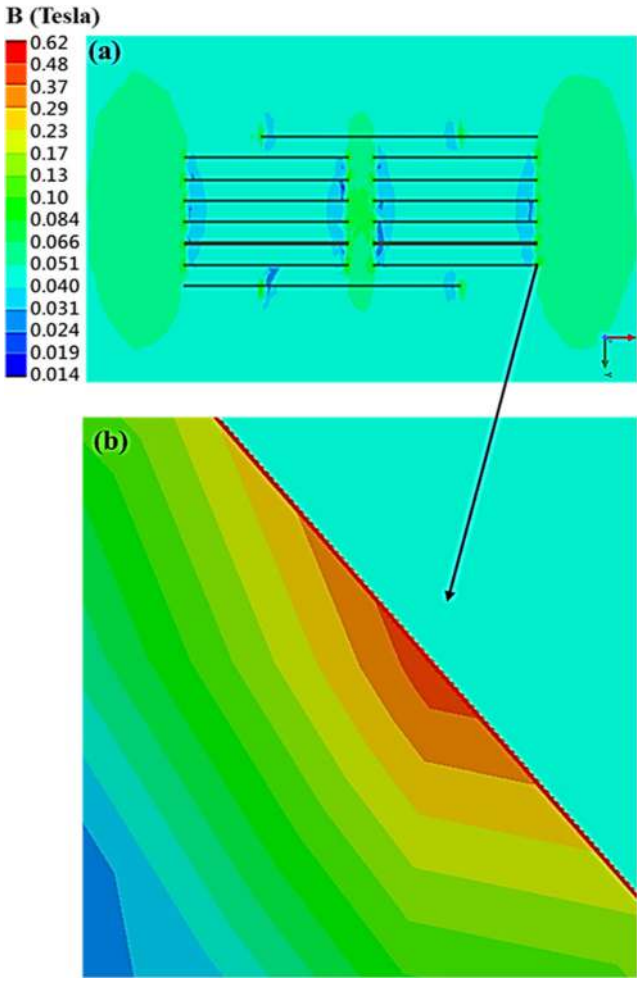

Fig. 13 **a** Distribution profile of the magnetic flux density around the surface of the Roebel cable at an applied field of 0.05 T. **b** Enlarged view of the lateral edge of a strand

It can be noticed that the magnetic flux density is high at the edge of the strand, and the intensity of magnetic field lines is minimum at the inside of the strand. The plot and magnetic field distribution obtained is similar to that presented in [26] in which a detailed description of the magnetic field around a Roebel cable is presented. For the same cable, the magnetic field applied to the broad face is then varied from 0.01 to 0.1 T, and the magnetic field distribution around the region of the Roebel cable is plotted and compared. The surface plot obtained gives a similar impression with the only variation in the magnitude of the maximum obtained magnetic field density.

The magnetic field distribution around the region of a real case Roebel cable for an applied field of 0.05 T is also plotted and shown in Fig. 14. A small variation can be noticed in the distribution profile of the magnetic flux density and the magnitude of maximum flux density. Due to the 3D structure and consideration of real case twisting of the strands of the Roebel cable, the magnetic field applied perpendicular to the broad face of the cable may not be perpendicular at all regions of the strand. Since geometry plays an important role in the response to a given magnetic field, there can be a slight variation in the

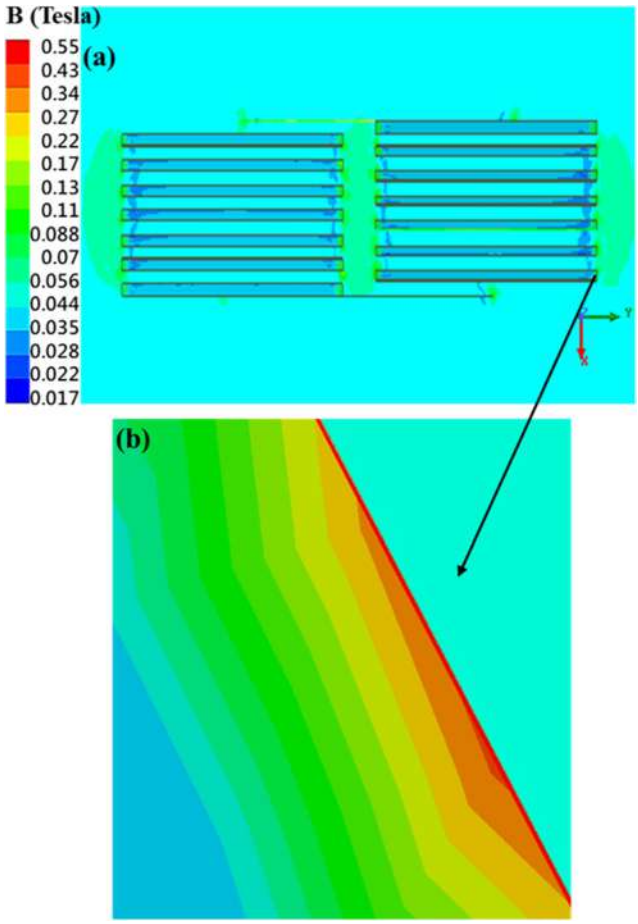

Fig. 14 **a** Distribution profile of magnetic flux density around the surface of a real case Roebel cable at an applied field of 0.05 T. **b** Enlarged view of the lateral edge of a strand

evaluated result. In this case, also the magnetic flux density is higher at the edges of the strand. However, the average magnetic flux density remains almost the same. Similar plots are evaluated for all applied fields (i.e. from 0.01 to 0.1 T); however, no differences are observed in the distribution profile, except for the magnitude of the maximum flux density that varies according to the applied field.

4.2 Transport Current

For analysing the magnitude of AC loss in the 14-strand Roebel cable when current passes through it, an alternating current of frequency 50 Hz varying from $0.1I_c$ to I_c is applied to the cable, where I_c is the critical current which is taken as 465 A. AC loss in the cable at various applied current vs relative transport current is shown in Fig. 15. Relative transport current is the ratio of the applied current to the critical current of the cable. The average of the analysed data obtained from the simulation against each applied current varying from $0.1I_c$ to I_c is taken for plotting the graph in the FEA case.

From Fig. 15, it can be inferred that the AC loss obtained via FEA is in good agreement with that of the data presented in [13] for an applied current from $0.4I_c$ to I_c. However, at low applied current (i.e. from $0.1I_c$ to $0.3\ I_c$), FEA underestimates the experimental result and the 3D power law.

The main reason for variation is because, in the experiment, the cable takes into account all the layers in it for calculating the AC loss and the frequency of the applied magnetic field was 72 Hz. However, in FEA, the loss is estimated only for the HTS layers and the strands are isolated individually, which the experiment overlooked. Even though in the graph the curve shows significant deviation, the value is minimal, which is in 10^{-4} range. It is due to the log scale representation of the graph; the deviation seems broad.

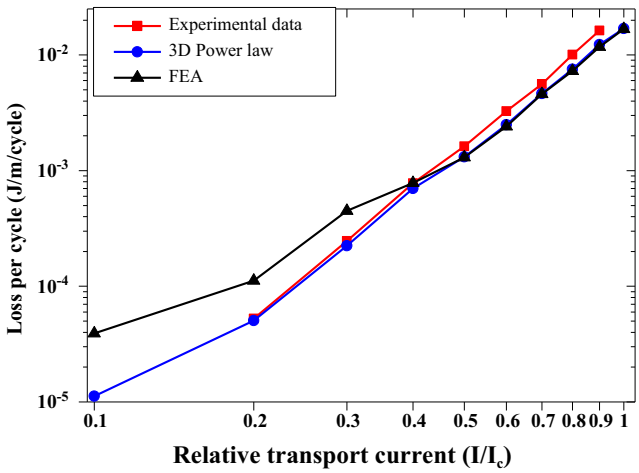

Fig. 15 Comparison between the AC loss data (for transport current case) obtained from various authors with respect to the FEA explained in this work. Experimental data were obtained from [15]. Curves indicated by power law were the data obtained from [13]

The main reason for slight deviation in the FEA result from the 3D power law is because, in the 3D power law, the model used for the simulation of the14-strand cable was the H-formulation technique that is commonly used for 2D problems. However, in this work, the 3D electromagnetic analysis is performed using the Maxwell equations available within the FEA tool. Also, in [13], the layer thickness of HTS has been scaled and reduced to 10 μm. The present work has overlooked such approximations as it would affect the distance between the HTS layer in each strand which may in turn affect the simulation result of the cable. In the current work, as an initial approach, the material properties are considered linear.

In order to visualise the variation of AC loss at different regions of the Roebel cable, the surface plot of the AC loss is investigated at different applied current values varying from $0.1I_c$ to I_c. The surface plot of the AC loss on a 14-strand Roebel cable applied with a current of $0.5I_c$ is illustrated in Fig. 16. In Fig. 16, one can notice that the loss is concentrated on the two sides of the strand. At the transposition section of the strand, the loss is minimal. The surface plot obtained in [13] shows a similar impression of the transport current case. It is found that the maximum AC loss for this instant is 7.6E −03 J/m/cycle and the average AC loss is 1.3E−03 J/m/cycle, which is comparable with what was mentioned in [13]. Similar plots are estimated from FEA for current values varying from $0.1I_c$ to I_c; all show similar outline with the only variation in the magnitude of the losses which will certainly change depending on the magnitude of applied current.

Figure 17 displays the simulated result of the current density distribution in a single strand detached from a 14-strand Roebel cable applied with a transport current of $0.5I_c$. It is noticed that the current density is maximum in the region where a sudden change in the direction of current occurs, i.e. at the beginning of the crossover section of the strand. At all other portions, the current density is almost uniform. The

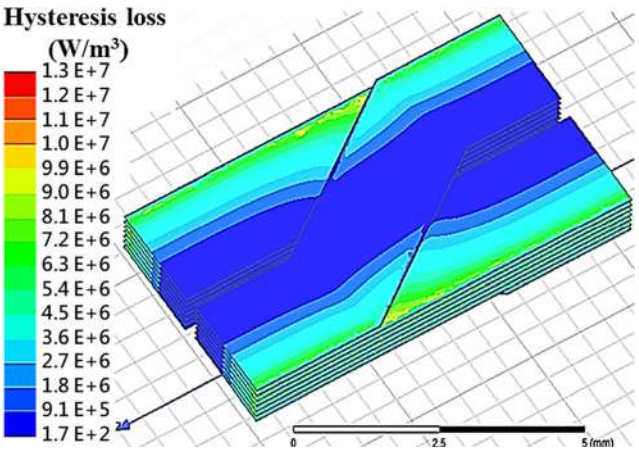

Fig. 16 Surface plot of the distribution of AC loss in a-14 strand Roebel cable at an applied transport current of $0.5I_c$

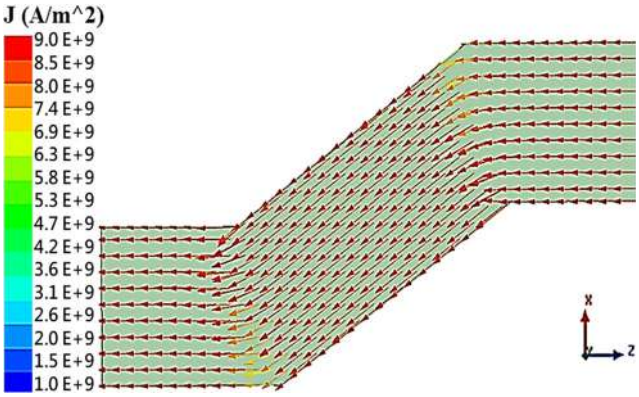

Fig. 17 Distribution of current density in the Roebel strand

average current density for the above situation is 8.3E9 A/m^2 which is precisely equal to the calculated current density, which indicates that the simulation results are correct. A similar plot can be generated for any strand in the Roebel cable, and the intensity of the current density and its region of maxima and minima in each strand can be visualised for any applied current. It is a point to be noted that most of the current density vectors are transmitted along the periphery of the strand which is in contact with the air which shows an exact similar profile as mentioned in [13, 19]. For any applied current that varies from 0.1I_c to I_c, the vector distribution profile of the current density in the Roebel cable is identical; only the variation is noted in the magnitude of the current density.

AC loss analysis is also performed on a real case Roebel cable that considers the strand's natural twist. The obtained AC loss is then compared with the Roebel cable in which the strands are considered straight and presented in Fig. 18. No difference is observed on the surface plot at any applied current except in the magnitude of the AC losses. It is interesting to note that the AC loss obtained for the real case Roebel cable is lower than the other for all applied current values. It is also

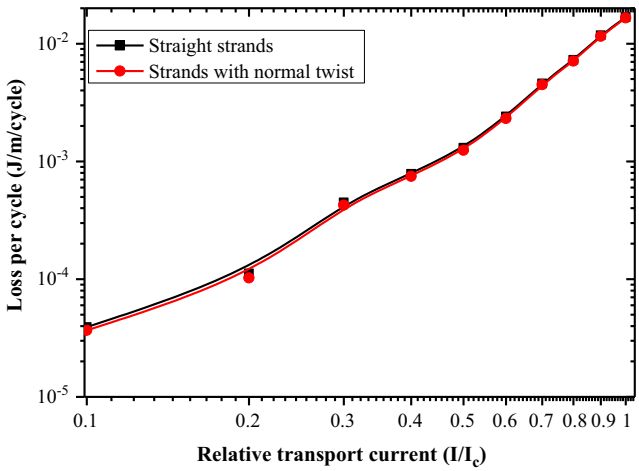

Fig. 18 Comparison between the AC losses per cycle in a 14-strand Roebel cable (where the strand in it is considered straight) and real case Roebel cable

noticed that the variation in AC loss at low applied current is significant compared with the high applied current, i.e. the variation in AC loss between the real case Roebel cable and the other reduces when the applied current increases gradually from 0.1I_c to I_c. The difference between the AC loss at all applied current (i.e. from 0.1I_c to I_c) is estimated for both cables, and the average AC loss reduction from 0.1I_c to I_c is found to be 4.13%.

Vector representation of the current density distribution profile of a strand separated from a real case 14-strand Roebel cable applied with a current of 0.5I_c is evaluated and presented in Fig. 19. The obtained distribution profile for all applied current varying from 0.1I_c to I_c is also the same; the only variation is noted in the magnitude of the current density. It can be visualised that there is no remarkable variation between the distribution profile of straight strand and twisted strands of the Roebel cable. Nonetheless, one may note that the average current densities for the applied transport currents remain the same, but the maximum current densities reached in both cases vary. The maximum current density for the twisted strand is less for the same current applied, which means more current can be transferred through the cable if the strands in the cables are twisted [15].

The magnetic field intensity distribution profile around the region of a Roebel cable with a strand considered straight and twisted is also plotted for an applied current of 0.5I_c and presented in Figs. 20 and 21 respectively. The intensity of magnetic field is high at the lateral edges of each strand in the Roebel cable. It may be noted that although wide variation is not found in the surface plot of the magnetic field intensity around the region of Roebel cables, the magnitude of peak magnetic field intensity obtained is a little high in the latter case. Similar plots are evaluated for all applied current varying from 0.1I_c to I_c, but the distribution profile shows no variations except for the magnitude of the maximum flux density that varies according to the applied current.

The geometry (3D model) plays a crucial role in the magnetic field intensity distribution around a conductor [19]. In real case Roebel cable, there is a variation in the geometry due

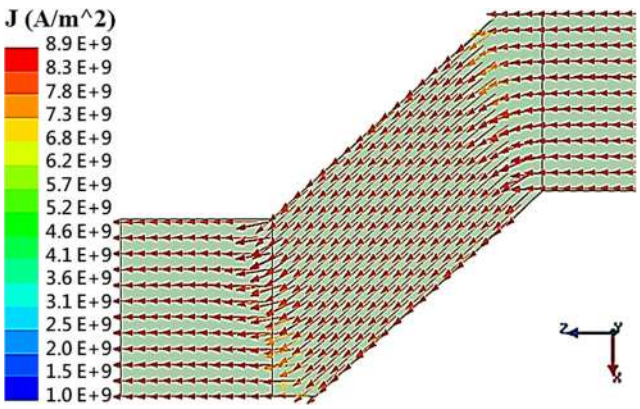

Fig. 19 Distribution of current density in the real case Roebel strand

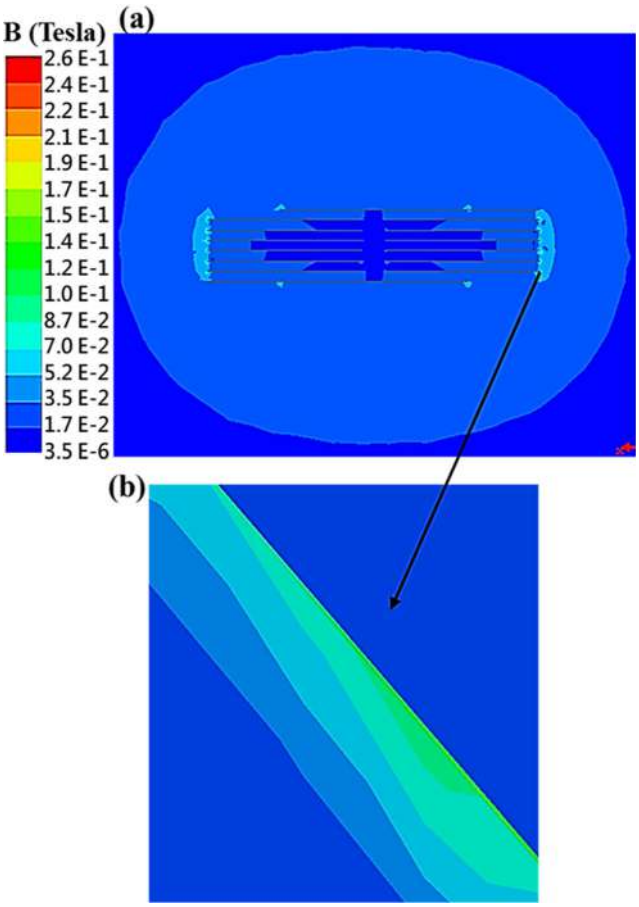

Fig. 20 **a** Magnetic field intensity distribution profile around the region of the Roebel cable (strand considered straight). **b** Enlarged view of the lateral edge of a strand

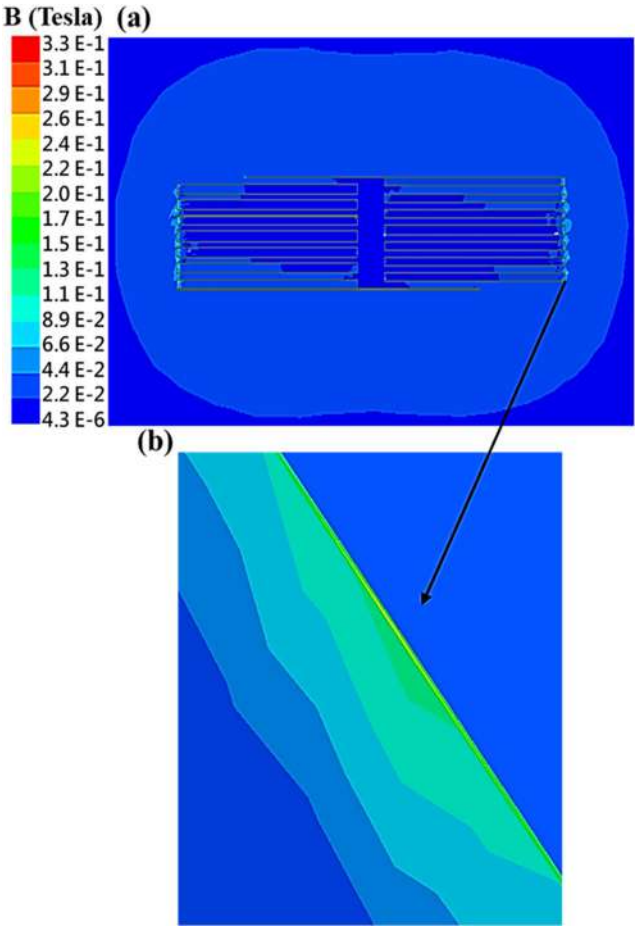

Fig. 21 **a** Magnetic field intensity distribution profile around the region of real case Roebel cable (strand's natural twisting considered). **b** Enlarged view of the lateral edge of a strand

to the consideration of the strand's natural twisting, which is the main reason for a slight variation in the surface plot obtained.

5 Conclusion

In this work, the AC loss analysis, the current distribution in strands and the magnetic field distribution are evaluated in a 14-strand HTS Roebel cable using finite element method in two cases: (i) AC magnetic field applied to HTS Roebel cable and (ii) AC passes through HTS Roebel cable. The results were then compared with the numerical results presented in [13]. The analysis is also performed on a real case Roebel cable that considers strand's natural twist. This small distortion may arise due to the transposition of one strand over the other during cable manufacturing.

In the first case, no significant variation is noticed between FEA and power law in the AC loss except at extremely low magnetic field. However, during the second case, the FEA results underestimated the power law at low applied current even though a good agreement is shown for large applied current. Even though minute variation is noted between the experimental data, power law and FEA, the overall trend is reproduced. For the first case, the loss is concentrated at the transposition section of the strand. At the straight sections, losses are almost the same. The current density is high at the edge and also at the crossover region of the strand. The magnetic flux density is high at the edge of the strand, and the intensities of magnetic field lines are minimum at the inside of the strands. For the second case, the AC loss concentrates on the two sides of the strand. At the transposition section of the strand, the loss is minimal. The current density is maximum in the region where a sudden change in the direction of current occurs, i.e. at the beginning of the crossover section of the strand. At all other portions, the current density is almost uniform. The intensity of magnetic field is high at the lateral edges of each strand in the Roebel cable.

In comparing the Roebel cable having straight strands with real case Roebel cable, for the first case, the variation of AC loss between both is negligibly small. However, the maximum current density increases and the maximum magnetic flux density (around the region of the cable) reduces if we consider

the natural twisting of the strand even though the average of both remains the same in the cable. In the second case, it is interesting to note that the AC loss obtained in real case 3D Roebel cable is lower than the other for all applied current values. The average AC loss reduction from $0.1I_c$ to I_c is found out to be 4.13%. The maximum current density and the maximum magnetic flux density (around the region of the cable) increased when the natural twisting of the strand is considered. This is an indication that geometry plays an important role in the distribution of current density and magnetic field variation in and around a superconductor in response to the applied current and magnetic field. Comparing the obtained surface plots (AC loss, current density distribution profile, the magnetic field around the cable) of the straight-stranded Roebel cable with real case 3D Roebel cable, for the first case and the second case, it looks similar. The variation in the applied magnetic field or current causes no significant variation in the obtained surface plot (AC loss, current density or magnetic field around the cable) either in a straight-stranded Roebel cable or in real case Roebel cable, except for the magnitude of the above parameters.

The main reason for slight deviation in the FEA result from [13] is because, in the 3D power law, the model used for the simulation of a 14-strand cable was the H-formulation technique that is commonly used for 2D problems. However, in this work, the 3D electromagnetic analysis is performed using the Maxwell equations available within the FEA tool. Also, in [13], the layer thickness of HTS has been scaled and reduced. The present work has overlooked such approximations as it would affect the distance between the HTS layer in each strand which may affect the simulation result of the cable. In the present work, the material properties are considered linear as an initial approach. These discrepancies will be avoided in future work where the material's nonlinear properties will be considered. Although several numerical simulations have been carried out to optimise the HTS Roebel cable, no work has yet been conducted on the 3D finite element analysis and simulation of the complete 3D structure of the Roebel cable. This work can therefore be considered as an initiator for the 3D finite element electromagnetic analysis of HTS Roebel cables.

Acknowledgements We acknowledge the Space Technology Laboratory under the Department of Mechanical Engineering, TKM College of Engineering, Karikode, Kollam, Kerala, India, for providing the computational facilities.

References

1. Wilson, M.N.: Superconductivity and accelerators: the good companions. IEEE Trans. Appl. Supercond. **9**, 111–121 (1999)
2. Goldacker, W., Nast, R., Kotzyba, G., Schlachter, S.I., Frank, A., Ringsdorf, B., Schmidt, C., Komarek, P.: High current DyBCO-ROEBEL assembled coated conductor (RACC). J. Phys. Conf. Ser. **43**, 901–904 (2006)
3. Fleiter, J., Ballarino, A., Bottura, L., Goldacker, W., Kario, A.: Characterization of roebel cables for potential use in high-field magnets. IEEE Trans. Appl. Supercond. **25**, 3–6 (2015)
4. Barth, C.: High temperature superconductor cable concepts for fusion magnets. KIT Scientific Publishing. **7**, (2013)
5. Grilli, F., Zermeno, V.M.R.: Effect of tape's Ic inhomogeneity and strand misalignment on the transport capacity of Roebel cables. IEEE Trans. Appl. Supercond. **27**, 1–5 (2017)
6. Goldacker, W., Grilli, F., Pardo, E., Kario, A., Schlachter, S.I., Vojenčiak, M.: Roebel cables from REBCO coated conductors: a one-century-old concept for the superconductivity of the future. Supercond. Sci. Technol. **27**, 093001 (2014)
7. Goldacker, W., Frank, A., Kudymow, A., Heller, R., Kling, A., Terzieva, S., Schmidt, C.: Status of high transport current ROEBEL assembled coated conductor cables. Supercond. Sci. Technol. **22**, 034003 (2009)
8. Wang, M., Zhang, M., Song, M., Li, Z., Dong, F., Hong, Z., Jin, Z.: An effective way to reduce AC loss of second-generation high temperature superconductor. Supercond. Sci. Technol. **32**, 01LT01 (2018)
9. Li, Z., Hu, D., Zhang, L., Xie, Z., Sun, L., Liu, B., Hong, Z., Jin, Z., Ryu, K.: Development of a novel soldered-stacked-square (3S) HTS wire using 2G narrow tapes with 1 mm width. IEEE Trans. Appl. Supercond. **27**, 6600904 (2017)
10. Li, Y., Hao, J., Liu, H., Li, Y., Ma, Y.: The metallization and superconductivity of dense hydrogen sulfide. J. Chem. Phys. **140**, 174712 (2014)
11. Drozdov, A.P., Kong, P.P., Minkov, V.S., Besedin, S.P., Kuzovnikov, M.A., Mozaffari, S., Balicas, L., Balakirev, F.F., Graf, D.E., Prakapenka, V.B., Greenberg, E., Knyazev, D.A., Tkacz, M., Eremets, M.I.: Superconductivity at 250 K in lanthanum hydride under high pressures. Nature. **569**, 528–531 (2019)
12. Bergen, A., Andersen, R., Bauer, M., Boy, H., ter Brake, M., Brutsaert, P., Bührer, C., Dhallé, M., Hansen, J., ten Kate, H., Kellers, J., Krause, J., Krooshoop, E., Kruse, C., Kylling, H., Pilas, M., Pütz, H., Rebsdorf, A., Reckhard, M., Seitz, E., Springer, H., Song, X., Tzabar, N., Wessel, S., Wiezoreck, J., Winkler, T., Yagotyntsev, K.: Design and in-field testing of the world's first ReBCO rotor for a 3.6 MW wind generator. Supercond. Sci. Technol. **32**, 125006 (2019)
13. Zermeno, V.M.R., Grilli, F., Sirois, F.: A full 3D time-dependent electromagnetic model for Roebel cables. Supercond. Sci. Technol. **26**, 052001 (2013)
14. Ilin, K., Yagotintsev, K.A., Zhou, C., Gao, P., Kosse, J., Otten, S.J., Wessel, W.A.J., Haugan, T.J., Van Der Laan, D.C., Nijhuis, A.: Experiments and FE modeling of stress-strain state in ReBCO tape under tensile, torsional and transverse load. Supercond. Sci. Technol. **28**, 055006 (2015)
15. Terzieva, S., Vojenčiak, M., Pardo, E., Grilli, F., Drechsler, A., Kling, A., Kudymow, A., Gömöry, F., Goldacker, W.: Transport and magnetization ac losses of ROEBEL assembled coated conductor cables: measurements and calculations. Supercond. Sci. Technol. **23**, 014023 (2010)
16. Hazelton, D. W.: Progress in coated conductor at SuperPower. SuperPower-inc. http://www.superpower-inc.com/content/technical-documents (2010)
17. Nii, M., Amemiya, N., Nakamura, T.: Three-dimensional model for numerical electromagnetic field analyses of coated superconductors and its application to Roebel cables. Supercond. Sci. Technol. **25**, 095011 (2012)
18. Goldacker, W., Frank, A., Kudymow, A., Heller, R., Kling, A., Terzieva, S., Schmidt, C.: Improvement of superconducting properties in ROEBEL assembled coated conductors (RACC). IEEE Trans. Appl. Supercond. **19**, 3098–3101 (2009)

19. Grilli, F., Pardo, E., Stenvall, A., Nguyen, D.N., Yuan, W., Gomory, F.: Computation of losses in HTS under the action of varying magnetic fields and currents. IEEE Trans. Appl. Supercond. **24**, 78–110 (2013)
20. Van Nugteren, J., Van Nugteren, B., Gao, P., Bottura, L., Dhallé, M., Goldacker, W., Kario, A., Ten Kate, H., Kirby, G., Krooshoop, E., De Rijk, G., Rossi, L., Senatore, C., Wessel, S., Yagotintsev, K., Yang, Y.: Measurement and numerical evaluation of AC losses in a ReBCO Roebel Cable at 4.5 K. IEEE. Trans. Appl. Supercond. **26**, 8201407 (2016)
21. Knizhnik, A., Shter, G.E., Grader, G.S., Reisner, G.M., Eckstein, Y.: Interrelation of preparation conditions, morphology, chemical reactivity and homogeneity of ceramic YBCO. Phys. C. Supercond. Appl. **400**, 25–35 (2003)
22. Talisa, S.H., Janocko, M.A., Moskowitz, C., Talvacchio, J., Billing, J.F., Brown, R., Buck, D.C., Member, S., Jones, C.K., Mcavoy, B.R., Wagner, G.R., Watt, D.H.: Low- and high-temperature superconducting microwave filters. IEEE. Trans. Microw. Theory. Tech. **39**, 1448–1454 (1991)
23. Sarmago, R.V., Singidas, B.G.: Low field AC susceptibility of YBCO: the frequency and field dependence of intra- and intergrain coupling losses in the absence of vortices. Supercond. Sci. Technol. **17**, S578 (2004)
24. Lundy, D.R., Swartzendruber, L.J., Bennett, L.H.: Brief review of recent superconductivity research at NIST. J. Res. Natl. Inst. Stand. Technol. **94**, 147–178 (1989)
25. Nose, T., Yamaguchi, T., Yamamoto, M., Shiraishi, K., Shiraishi, T., Koinuma, H.: Magnetic permeability and antiferromagnetism of YBCO superconductors. J Adv Sci. **2**, 108–111 (1990)
26. Grilli, F., Pardo, E.: Simulation of ac loss in Roebel coated conductor cables. Supercond. Sci. Technol. **23**, 115018 (2010)